Morphological segmentation of physiographic features from DEM

D. Sathymoorthy[a]; R. Palanikumar[b]; B. S. D. Sagar[c]

[a] Science and Technology Research Institute Technology for Defence (STRIDE), D/A KD Malaya, 32100 Lumat, Perak, Malaysia [b] College of Computer Science, King Khalid University, Kingdom of Saudi Arabia [c] Faculty of Engineering and Technology (FET), Melaka Campus, Multimedia University, 75450, Melaka, Malaysia

PLEASE SCROLL DOWN FOR ARTICLE

Taylor & Francis
Taylor & Francis Group

Morphological segmentation of physiographic features from DEM

D. SATHYMOORTHY†, R. PALANIKUMAR*‡ and B. S. D. SAGAR§

†Science and Technology Research Institute Technology for Defence (STRIDE), D/A
KD Malaya, Pangkalan TLDM, 32100 Lumat, Perak, Malaysia
‡College of Computer Science, King Khalid University, PO Box 641 ABHA, Kingdom
of Saudi Arabia
§Faculty of Engineering and Technology (FET), Melaka Campus, Multimedia
University, Jalan Ayer Keroh Lama, 75450, Melaka, Malaysia

A terrain can be segmented into three predominant physiographic features;
mountains, basins and piedmont slopes. The objective of this paper is to develop
a mathematical morphological based algorithm to segment the terrain of a digital
elevation model (DEM) into the three predominant physiographic features.
Ultimate erosion is used to extract the peaks and pits of the DEM. Conditional
dilation is performed on the peaks and pits of the DEM to extract the mountain
and basin pixels, respectively. The unclassified pixels are assigned as piedmont
slope pixels. The combination of the mountain, basin and piedmont slope regions
form the physiographically segmented DEM. The effectiveness of the proposed
physiographic segmentation algorithm is tested by implementing it on the Global
Digital Elevation Model (GTOPO30) of the Great Basin, Nevada, USA.

1. Introduction

Physiography (also known as land surface characteristics) is the study of the
physical features and attributes of the Earth's land surface. The detection of the
physiographic features of a terrain is the first phase involved in the classification of
the various landforms of the terrain. The mapping of physiographic features is
generally performed manually through fieldwork and visual interpretation of
topographic maps, which is a time consuming and labour intensive activity. It is
expected that an efficient automated method for the extraction of physiographic
features will allow the easier production of a physiographic database within
geographical information systems (GIS). Terrain can be segmented into three
predominant physiographic features; mountains, piedmont slopes and basins.

Mountains are the portions of terrain that are sufficiently elevated above the
surrounding land (greater than 300 m to 600 m) and have comparatively steep sides.
In a mountain, two parts are distinctive:

(1) The summit, the highest point (the peak) or the highest ridges.
(2) The mountainside, the part of a mountain between the summit and the foot
    (Bates and Jackson 1987).

Basins are topographic regions from which drainage networks receive runoff,
throughflow, and groundwater flow. All the surface land from the highest point of

---

land down to the stream bottom is considered as part of the drainage network's basin. Basins are generated through the receival of tributaries carried by drainage networks in landslope regions (Monkhouse 1965).

Piedmont slopes are the parts of the terrain that are not classified as mountains or basins. Piedmont slopes form either narrow rings surrounding mountain ranges or gently sloping plains in between a basin and a mountain or eroded mountain remnants surrounded by basins (Miliaresis and Argialas 1999).

In this paper, a mathematical morphological based algorithm to segment the terrain of a digital elevation model into the three predominant physiographic features is proposed. Mathematical morphology is a branch of image processing that deals with the extraction of image components that are useful for representation and description of region shape, such as boundaries, skeletons and convex hulls (Gonzalez and Woods 1993). Mathematical morphology is well suited to the processing of elevation data because in morphology, any image is viewed as a topographic surface, the grey level of a pixel standing for its elevation (Soille and Ansoult 1990). Hence, mathematical morphological operators are extremely useful and important in digital elevation model (DEM) analysis. The fundamental morphological operators are discussed in Matheron (1975), Serra (1982), and Soille (2003). Morphological operators generally require two inputs; the input image A, which can be in binary or greyscale form, and the kernel B, which is used to determine the precise effect of the operator.

2. The proposed physiographic segmentation algorithm

The gradient values of the features of interest are as follows:

- (a) mountains: above $6°$;
- (b) piedmont slopes: $3°$ to $6°$;
- (c) basins: below $3°$.

The gradient values of a terrain are usually minimized in the pits and peaks, in contrast to the usually steep valley sides or cliff sides. Hence, physiographic segmentation cannot be performed through thresholding of the gradient of the DEM. The physiographic segmentation algorithm developed is as follows.

2.1 *Peak and pit extraction using ultimate erosion*

The peaks of a terrain refer to the highest points of the mountains of the terrain while the pits of the terrain are the lowest points of the basins of the terrain. In DEMs, peaks are connected components that are completely surrounded by pixels of lower elevation while pits are connected components that are completely surrounded by pixels of higher elevation. The extraction of peaks and pits from DEMs is the first step in most techniques used to perform DEM characterization, and to describe the general geomorphometry of a surface.

Dilation sets the pixel values within the kernel to the maximum value of the pixel neighbourhood. The dilation operation is expressed as:

$$A \oplus B = \{a + b;\ a \in A,\ b \in B\} \tag{1}$$

Erosion sets the pixels values within the kernel to the minimum value of the kernel. Erosion is the dual operator of dilation:

$$A \ominus B \subset (A^c \oplus B)^c \tag{2}$$

Greyscale erosion can be used to remove bright areas in greyscale images. It causes small peaks in the image to disappear. However, it also causes valley widening, which results in the formation of larger peaks.

Morphological reconstruction allows for the isolation of certain features within an image based on the manipulation of a mask image X and a marker image Y. It is founded on the concept of geodesic transformations, where dilations or erosion of a marker image are performed until stability is achieved (represented by a mask image) (Vincent 1993).

The geodesic dilation δ^G used in the reconstruction process is performed through iteration of elementary geodesic dilations $\delta_{(1)}$ until stability is achieved:

$$\delta^G(Y) = \delta_{(1)}(Y) \ o \ \delta_{(1)}(Y) \ o \ \delta_{(1)}(Y) \ldots \text{until stability} \tag{3}$$

The elementary dilation process is performed using standard dilation of size one followed by an intersection.

$$\delta_{(1)}(Y) = Y \oplus B \cap X \tag{4}$$

The operation in equation (4) is used for elementary dilation in binary reconstruction. In greyscale reconstruction, the intersection in the equation is replaced with a pointwise minimum (Vincent 1993).

Morphological reconstruction can be used to maintain the peak removal effect of erosion while avoiding the valley enlargement effect. The peaks removed by erosion can be obtained by subtracting the reconstructed eroded image from the original image. In order to extract the peaks of a DEM, ultimate erosion is performed on the DEM. Ultimate erosion is implemented by successively eroding an image until all particles vanish and performing morphological greyscale reconstruction on each eroded image into the erosion of smaller size (Duchene and Lewis 1996). Figure 1 demonstrates the operation of ultimate erosion. The generated ultimate eroded set of the DEM forms the peaks of the DEM. The pits of the DEM are the peaks of the inverted DEM; pit extraction is implemented by performing ultimate erosion on the inverted DEM.

2.2 Mountain extraction

Step 1: Conditional dilation of the peaks of the DEM.

The extracted peaks are dilated with a size 3 square kernel. The boundary pixels of the dilated peaks that have a gradient less than 6° are deleted. The conditional dilation of the peaks is repeated until no further changes are produced. In the image produced from this step, the foreground pixels are mountain pixels while the background pixels are non-mountain pixels.

Step 2: Removal of small islands of non-mountain pixels observed on mountain tops.

These pixels are flat to gently sloping regions, so the gradient was less than 6°. These pixels were not classified as peaks and Step 1 did not flag them as mountain pixels due to their gradient being less than 6°. However, these pixels have the geometric proximity to be mountain pixels. These erroneous non-mountain pixels are removed by assigning them as mountain pixels.

Step 3: Removal of small islands of mountain pixels observed in flat areas.

In flat areas, the noise (mean error in elevation) to signal (elevation) ratio is high, causing the formation of spurious peaks and pits. Spurious peaks cause the formation of erroneous mountain regions. These spurious peaks did not form larger mountain

When a particle disappears after an erosion, it is not reconstructed and thus appears in image U_i-

X_0 = input image

$X_1 = E[X_0]$

Y_0 = Reconstruction of X_0 using X_1

$U_0 = X_0-Y_0$

$X_2 = E[X_1]$

Y_1 = Reconstruction of X_1 using X_2

$U_1 = U_0\cup(X_1-Y_1)$

$X_3 = E[X_2]$

Y_2 = Reconstruction of X_2 using X_3

$U_2 = U_1\cup(X_2-Y_2)$

$X_4 = E[X_3] = \phi$

Y_3 = Reconstruction of X_3 using X_4
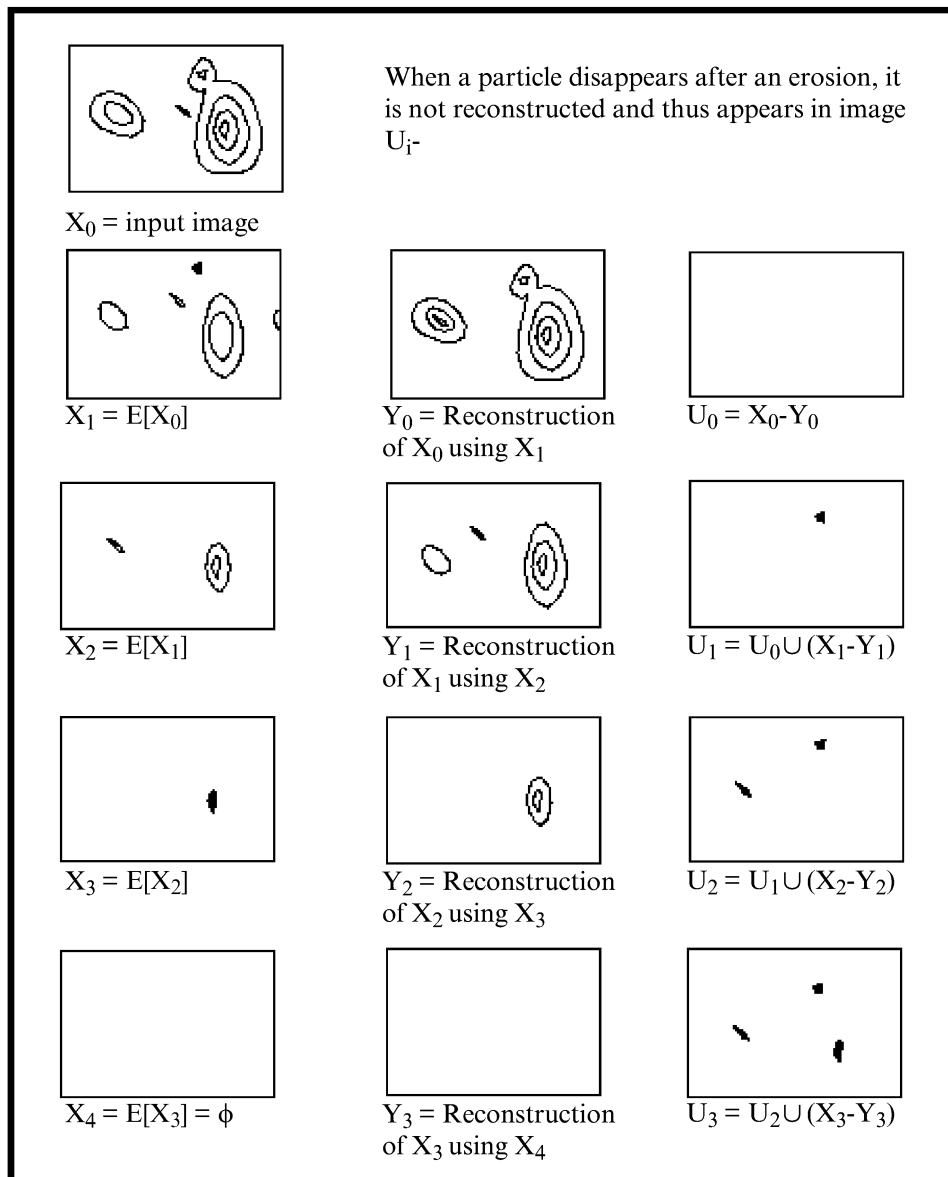
$U_3 = U_2\cup(X_3-Y_3)$

Figure 1. An example of the ultimate erosion operation. Ultimate erosion is implemented through the iterative erosion of the image until all objects vanish (images X_i), and the reconstruction of each eroded image using the eroded image, $E(X_i)$, as the mask and the erosion of smaller size as the marker. The reconstructed images (images Y_i) are subtracted from the corresponding eroded images to form the eroded sets (images U_i). The final resultant image is known as the ultimate erode set. (Reproduced with permission from Duchene and Lewis © 1996 NOEIS.)

regions as there are small gradient values in their neighborhood. These erroneous mountain pixels are removed by converting them into non-mountain pixels.

2.3 Basin extraction

Step 1: Conditional dilation of the pits of the DEM.

For basin extraction, only the non-mountain pixels are considered. The extracted pits are dilated with a size 3 square kernel. The boundary pixels of the dilated pits that have gradient higher than 3° are deleted. The conditional dilation of the pits is repeated until no further changes are produced. In the image produced from this step, the foreground pixels are basin pixels while the background pixels are non-basin pixels.

Step 2: Removal of small islands of non-basin pixels enclosed within basin regions.

These pixels were not classified as pits and Step 1 did not flag them as basin pixels due to their gradient being more than 3°. However, these pixels have the geometric proximity to be basin pixels. These erroneous non-basin pixels are removed by assigning them as basin pixels.

Step 3: Removal of small islands of basin pixels observed in non-basin areas.

These erroneous basin regions are caused by spurious pits. Spurious pits did not form larger basin regions as there are large gradient values in their neighbourhood. These erroneous basin pixels are removed by converting them into non-basin pixels.
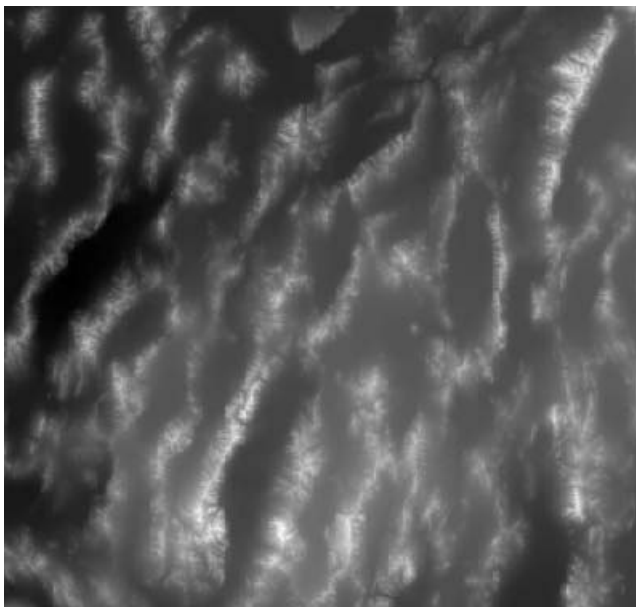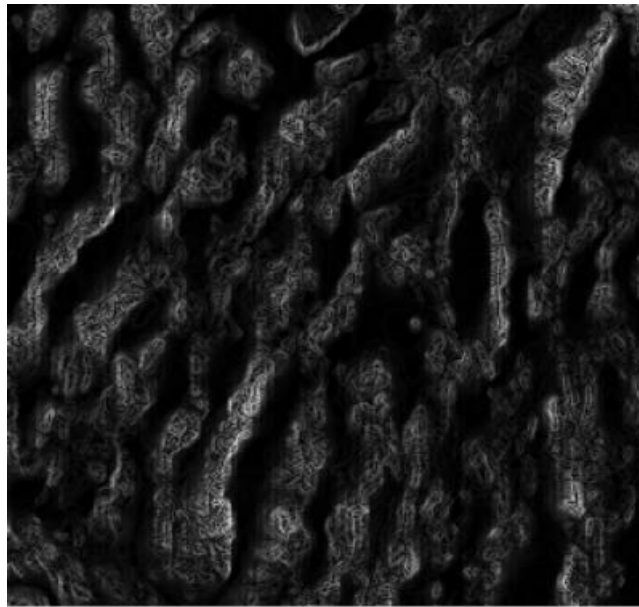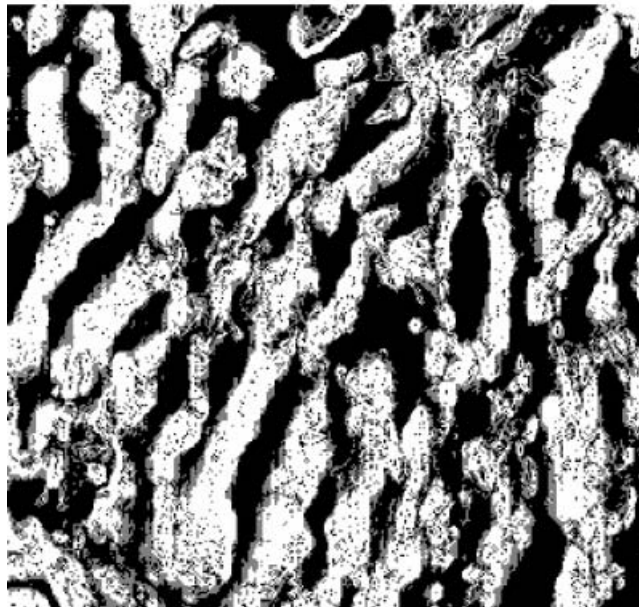

Figure 2. The GTOPO30 digital elevation model of Great Basin, Nevada, USA. The elevation values of the terrain (minimum 1005 m and maximum 3651 m) are rescaled to the 0–255 interval (the brightest pixel has the highest elevation). The scale is approximately 1 : 3 900 000.

(a)

(b)

Figure 3. Gradient analysis of the digital elevation model (DEM) of Great Basin, Nevada, USA. (a) The pixels of the DEM (in the gradient range of $0°$ to $57.12°$) rescaled to the 0–255 interval (the brightest pixel has the highest gradient). (b) Gradient thresholding of the DEM. The pixels in white have a gradient higher than $6°$, the pixels in grey have a gradient between $3°$ and $6°$ and the pixels in black have a gradient less than $3°$.
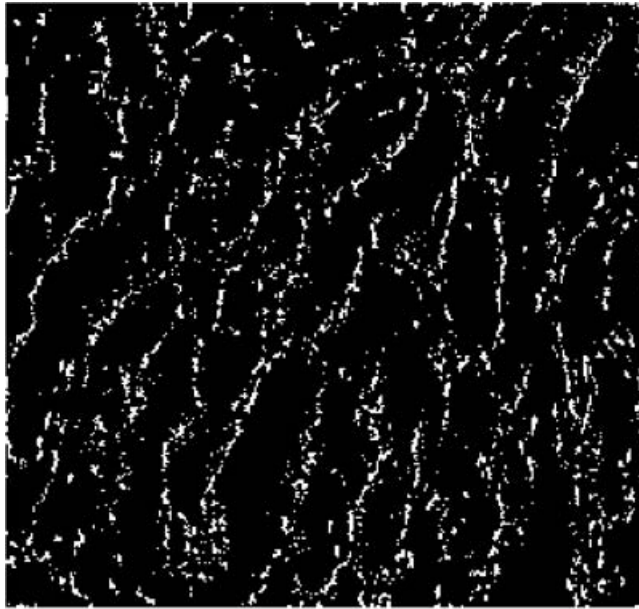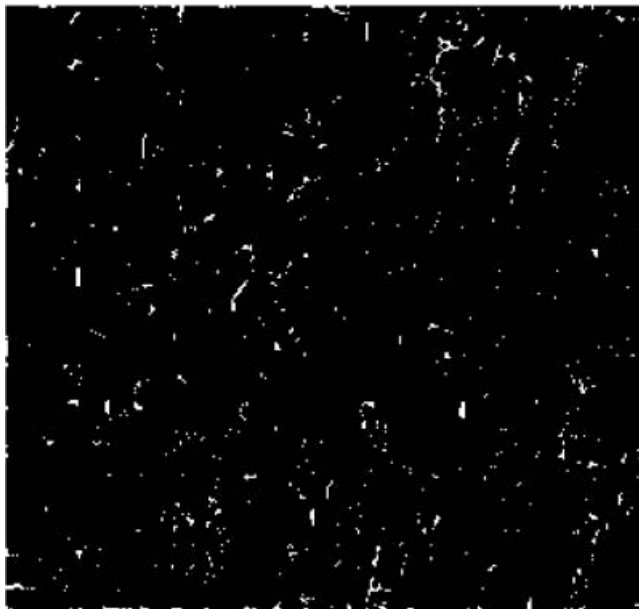
Figure 4. Extraction of (*a*) peaks and (*b*) pits from the digital elevation model of Great Basin, Nevada, USA.

(a)

(b)

Figure 5.   Mountain extraction. (a) The mountain pixels (the pixels in white) of the ditial elevation model. The black pixels are non-mountain pixels. (b) The mountain pixels after the removal of erroneous non-mountain regions enclosed by mountain pixels. (c) The mountain pixels after removal of erroneous mountain pixels. (d) The identification of the individual mountain objects.
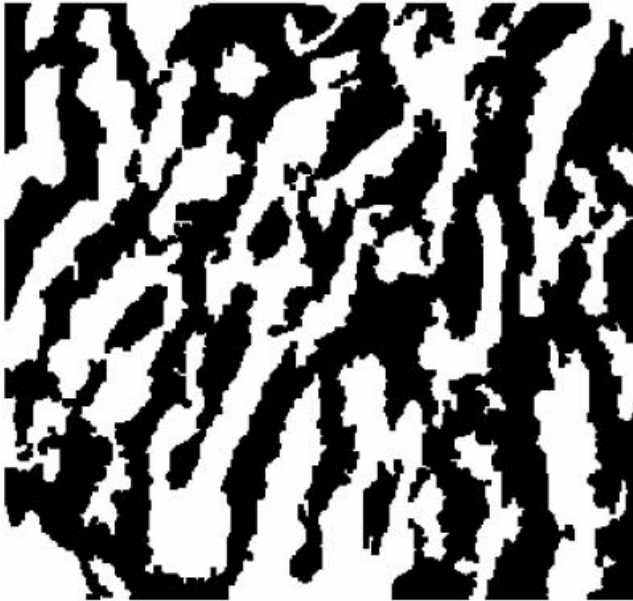
(*c*)
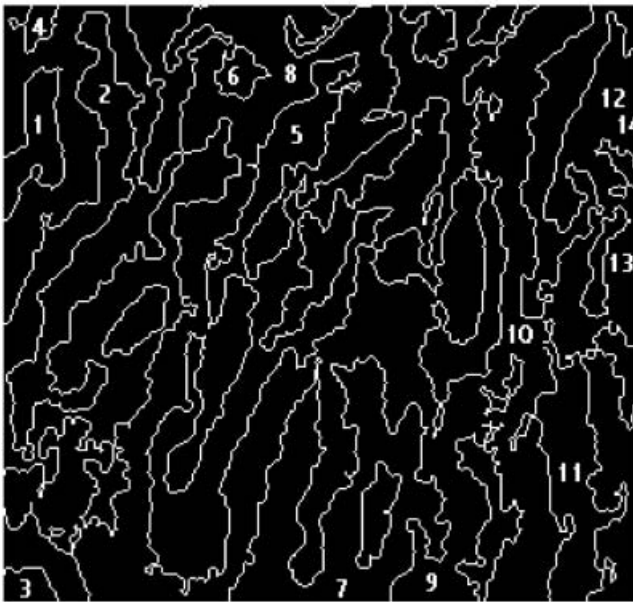
(*d*)

Figure 5. (*Continued.*)

2.4 *Piedmont slope pixels*

The pixels that are not assigned as mountain pixels or basin pixels were classified as piedmont slope pixels. The combination of the extracted mountains, basin and piedmont slope regions form the physiographically segmented DEM.

3. Case study

The DEM in figure 2 shows the area of Great Basin, Nevada, USA. The area is bounded by latitude 38°15′ to 42° N and longitude 118°30′ to 115°30′ W. The DEM was rectified and resampled to 925 m in both x and y directions. The DEM is a Global Digital Elevation Model (GTOPO30 DEM) and was downloaded from the United States Geological Survey (USGS) GTOPO30 website (http://edcwww. cr.usgs.gov/landdaac/gtopo30/gtopo30.html). GTOPO30 DEMs are available at a global scale, providing a digital representation of the Earth's surface at a 30 arc-s sampling interval. The land data used to derive GTOPO30 DEMs are obtained from digital terrain elevation data (DTED), the 1° DEM for USA and the digital chart of the world (DCW). The accuracy of GTOPO30 DEMs varies by location according to the source data. The DTED and the 1° dataset have a vertical accuracy of ± 30 m, while the absolute accuracy of the DCW vector dataset is ± 2000 m horizontal error and ± 650 vertical error (Miliaresis and Argialas 2002). The DEM of Great Basin has a mean gradient of 4.94. Figure 3(*a*) shows the pixels of the DEM in the gradient range of 0° to 57.12° rescaled to an interval of 0–255. The DEM contains 34 248 pixels (37.46%) with a gradient higher than 6°, 19 488 pixels (21.32%) with a gradient between 3° and 6° and 36 491 pixels (39.92%) with a gradient less than 3°. As shown in figure 3(*b*), the gradient thresholding of the DEM is an invalid physiographic segmentation method as it fails to classify the peaks and mountain-tops of the DEMs as mountain pixels (the pixels in white).

The proposed peak and pit extraction algorithm is implemented on the DEM of a total of 1315 peaks (figure 4(*a*)) and 559 pits are extracted from the DEM (figure 4(*b*)). A total of 6010 pixels (6.60%) are classified as peak pixels, while 1417 pixels (1.56%) are classified as pit pixels.

The conditional dilation process is repeated on the extracted peaks until convergence (figure 5(*a*)). The small islands of non-mountain pixels enclosed by mountain pixels are assigned as mountain pixels (figure 5(*b*)). The mountain regions with size less than 180 pixels are removed by converting these pixels to non-mountain pixels (figure 5(*c*)). A total of 42 168 pixels (46.13%) are classified as mountain class pixels. These pixels form 14 distinct mountain objects (figure 5(*d*)),

Table 1. Numerical description of the extracted mountains.

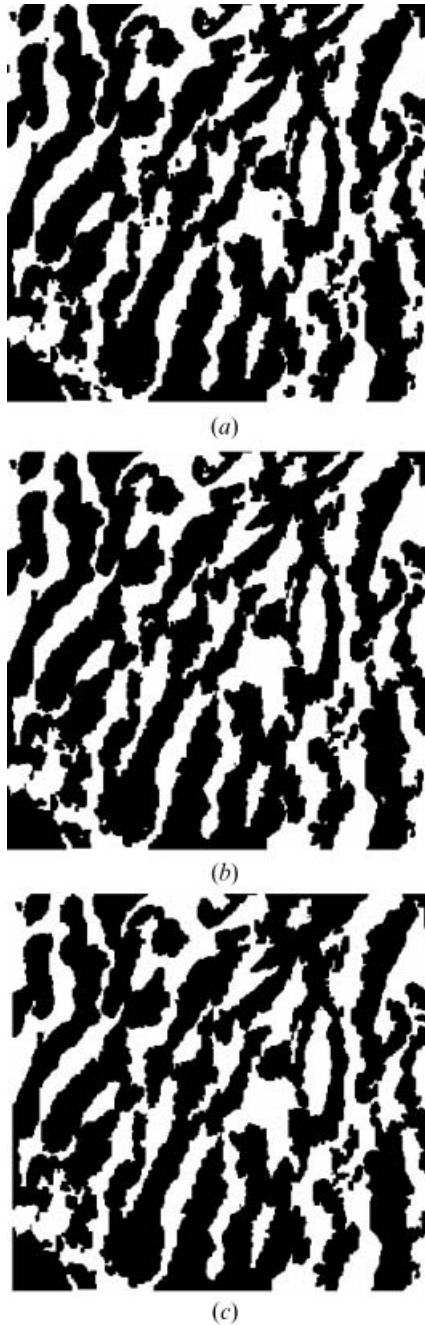| Object ID	Area (pixels)	Perimeter (pixels)	Maximum elevation (grey level)	Mean gradient (°)
1	1227	219	178	11.94
2	10 422	2 277	191	10.61
3	1 353	161	149	8.28
4	298	88	123	10.08
5	14 232	3 391	240	10.22
6	432	113	143	10.87
7	6 444	999	255	9.56
8	311	162	112	10.66
9	1 119	353	167	8.03
10	219	124	130	6.48
11	3 574	754	237	9.18
12	3 058	651	231	13.20
13	494	172	170	9.55
14	261	112	170	8.01

Figure 6.   Basin extraction. (*a*) The basin pixels (the pixels in white) of the DEM. The black pixels are non-basin pixels. (*b*) The basin pixels after the removal of erroneous non-basin regions enclosed by basin pixels. (*c*) The basin pixels after removal of erroneous basin pixels.

which are identified using the connected component labelling algorithm proposed in Pitas (1993). Each mountain object is described based on their size, perimeter, maximum elevation and mean gradient (table 1).
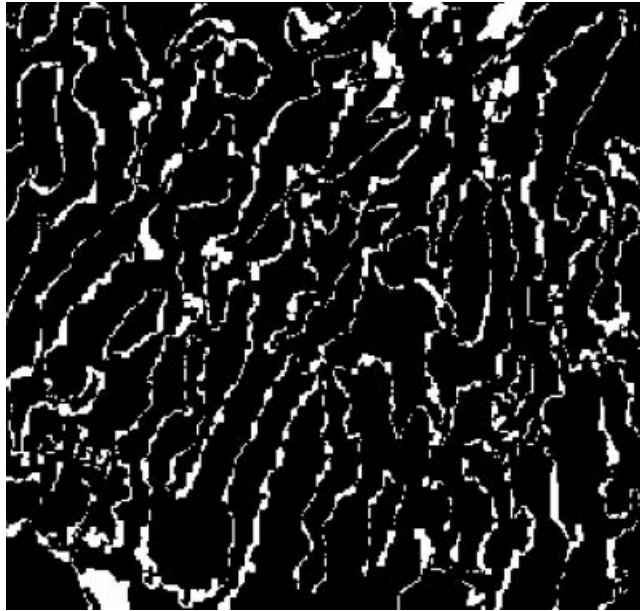
Figure 7.   The piedmont slope regions (the pixels in white).

The conditional dilation process is performed on the pits of the DEM until convergence (figure 6(*a*)). The small islands of non-basin pixels enclosed by basin pixels are assigned as basin pixels (figure 6(*b*)). The basin regions with size less than 180 pixels are removed by converting these pixels to non-basin pixels (figure 6(*c*)). A total of 36, 642 (40.21%) are classified as basin pixels.

The pixels that are not assigned as mountain pixels or basin pixels are assigned as piedmont slope pixels (figure 7). A total 11 037(12.11%) are classified as piedmont slope pixels. Figure 8(*a*) shows the generated physiographically segmented DEM.

In Miliaresis and Argialas (1999), physiographic segmentation of DEMs is performed by first extracting the seed ridge and valley pixels of the DEM using runoff simulation. The mountain regions are obtained by performing region growing on the seed ridge pixels and the basin pixels are obtained by performing region growing on the seed valley pixels. The pixels that were not classified as mountain or basin pixels are classified as piedmont slope pixels. The results obtained using this algorithm are shown in figure 8 (*b*). The algorithm resulted in 40 419 pixels (43.50%) being classified as mountain pixels, 26 835 (29%) pixels as basin pixels and 25 574 (27.5%) pixels as piedmont slope pixels. The mountain pixels formed 36 distinct mountain regions.

A good match was evident between the results obtained using the developed mathematical morphological based algorithm and the results obtained in Milaresis and Argialas (1999) although some differences exist. The mountain objects in figure 8(*a*) are wider than the corresponding mountain objects in figure 8(*b*). A number of single mountain objects in figure 8(*a*) appeared broken in figure 8(*b*), resulting in figure 8(*a*) having fewer distinct mountain objects than figure 8(*b*). This difference occurs because the seed ridge pixel image does not contain a number of the peaks of the terrain despite containing most of the highest points of the mountain regions. Hence, region growing on the seed ridge pixel image is unable to
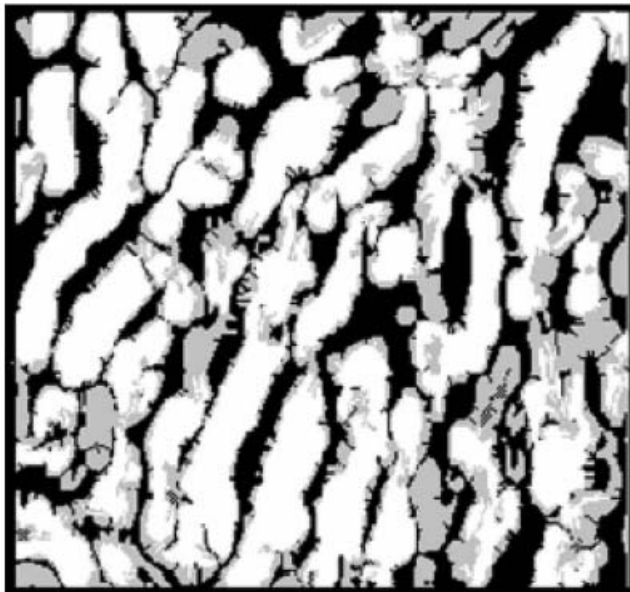
Figure 8. The mountain pixels are the pixels in white, the piedmont pixels are the pixels in grey and the basin pixels are the pixels in black. (*a*) The results obtained using the developed algorithm. (*b*) The results obtained in Miliaresis and Argialas (1999).

extract all of the mountain regions of the DEM, particularly the mountaintop regions.

The basin regions in figure 8(*b*) are smaller compared to figure 8(*a*). This difference occurs because the seed valley pixel image does not contain a number of
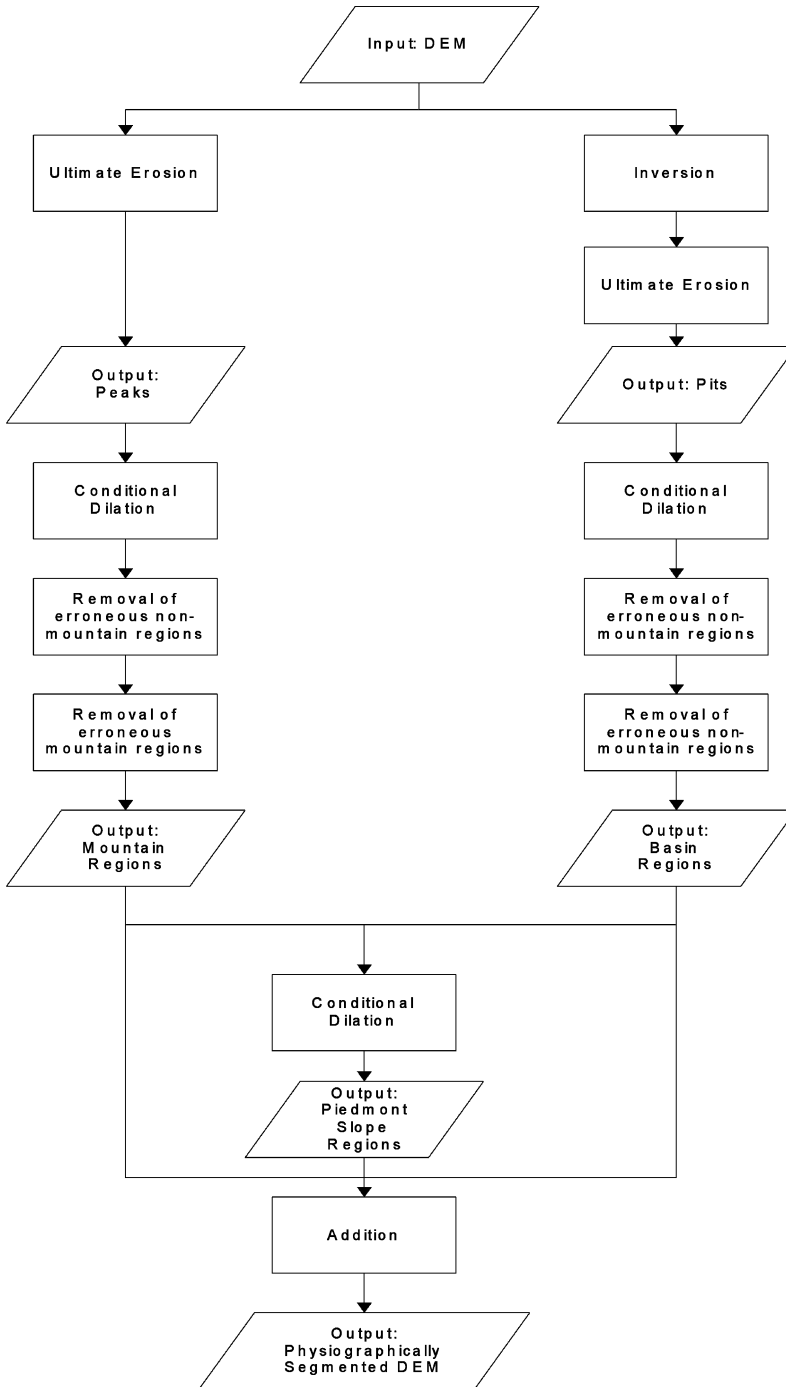
Figure 9.   The proposed physiographic segmentation algorithm.

the pits of the terrain despite containing most of the lowest points of the basin regions. Hence, region growing on the seed valley pixel image is unable to extract all of the basin regions of the DEM.

The disadvantage of the algorithm proposed in results obtained in Milaresis and Argialas (1999) is that runoff simulation is unable to operate effectively on flat areas in DEMs, resulting in errors in the extracted seed ridge and valley pixels, and hence causing errors in the extracted mountain and basin pixels. The proposed mathematical morphological based algorithm does not rely on flow directional based algorithms, and is able to operate effectively on flat areas in DEMs.

The differences observed were also due to the errors generated during the rescaling of the elevations (ranging between 1005 m to 3561 m) of the DEM to the 0–255 interval.

4. Conclusion

In this paper, a mathematical morphological based algorithm to segment the terrain of a DEM into the three predominant physiographic features, mountains, basins and piedmont slopes, was proposed. Ultimate erosion is used to extract the peaks and pits of the DEM. Conditional dilation is performed on the peaks and pits of the DEM to obtain the mountain and basin pixels, respectively. The pixels that are not classified as mountain pixels or basin pixels were assigned as piedmont slope pixels. The proposed physiographic segmentation algorithm summarized in the flowchart shown in figure 9 performs well in areas where a set of mountain features is developed in between basins standing at different base levels, and is able to operate effectively on the flat areas of DEMs.

In general, geomorphological landforms are viewed as Boolean objects. However, recent studies have shown that landforms are more suitable to be viewed as fuzzy objects, whereby a landform is defined as a region in the continuum of variation of the Earth's surface (Usery 1996, Fisher and Wood 1998, Burrough *et al.* 2000, 2001, Fisher 2000a,b, Varzi 2001, Fisher *et al.* 2004). At present, work is being done to perform the fuzzy classification of physiographic features extracted from multiscale DEMs.

References

BATES, R.L., and JACKSON, J.A. (Eds), 1987, *Glossary of Geology* (Alexandria, VA: American Geological Institute).

BURROUGH, P.A., VAN GAANS, P.F.M. and MACMILLAN, R.A., 2000, High-resolution landform classification using fuzzy k-means. *Fuzzy Sets and Systems*, **113**, pp. 37–52.

BURROUGH, P.A., WILSON, J.P., VAN GAAS, P.F.M. and HANSEN, A.J., 2001, Fuzzy k-means classification of topo-climatic data as an aid to forest mapping in the Greater Yellowstone Area, USA. *Landscape Ecology*, **16**, pp. 523–546.

DUCHENE, P. and LEWIS, D., 1996, Visilog 5 Documentation. Noesis Vision Inc., Quebec, Canada.

FISHER, P., 2000a, Fuzzy modeling. In *Geocomputing*, S. Openshaw, R. Abrahart and T. Harris (Eds), pp. 161–186 (London: Taylor and Francis).

FISHER, P., 2000b, Sorites paradox and vague geographies. *Fuzzy Sets and Systems*, **113**, pp. 7–18.

FISHER, P. and WOOD, J., 1998, What is a mountain? Or the Englishman who went up a Boolean geographical concept but realised it was fuzzy. *Geography*, **83**, pp. 247–256.

FISHER, P., WOOD, J. and CHENG, T., 2004, Where is Helvellyn? Fuzziness of multiscale landscape morphometry. *Transactions of the Institute of British Geographers*, **29**, pp. 106–128.

GONZALEZ, R.C. and WOODS, R.E., 1993, *Digital Image Processing* (New York: Addison-Wesley).

MATHERON, G., 1975, *Random Sets and Integral Geometry* (New York: John Wiley).

MILIARESIS, G.C., 2000, The DEM to mountain transformation of Zagros Ranges. *Proceedings 5th International Conference on GeoComputation*, 23–25 August 2000, University of Greenwich. Available online at http://hydrogis.geology.upatras.gr/_PAPERS.HTM.

MILIARESIS, G.C. and ARGIALAS, D.P., 1999, Segmentation of physiographic features from Global Digital Elevation Model/GTOPO30. *Computers & Geosciences*, **25**, pp. 715–728.

MILIARESIS, G.C. and ARGIALAS, D.P., 2002, Quantitative representation of mountain objects extracted from the Global Digital Elevation Model (GTOPO30). *International Journal of Remote Sensing*, **23**, pp. 949–964.

MONKHOUSE, F.J., 1965, *Principles of Physical Geography* (New York: University of London Press Ltd).

PITAS, I., 1993, *Digital Image Processing Algorithms* (London: Prentice Hall).

SERRA, J., 1982, *Image Analysis and Mathematical Morphology* (London: Academic Press).

SOILLE, P., 2003, *Morphological Image Analysis: Principles and applications* (Berlin: Springer Verlag).

SOILLE, P. and ANSOULT, M.M., 1990, Automated basin delineation from digital elevation models using mathematical morphology. *Signal Processing*, **20**, pp. 171–182.

USERY, E.L., 1996, A conceptual framework and fuzzy set implementation for geographic features. In *Geographic Objects with Indeterminate Boundaries*, P. Burrough and A. Frank (Eds), pp. 87–94 (London: Taylor & Francis).

VARZI, A.C., 2001, Vagueness in geography. *Philosophy and Geography*, **4**, pp. 49–65.

VINCENT, L., 1993, Morphological reconstruction in image analysis: applications and efficient algorithms. *IEEE Transactions on Image Processing*, **2**, pp. 176–201.